CONFOCAL MICROSCOPY PROVIDES A RAPID INTRAOPERATIVE HISTOLOGICAL ASSESSMENT OF BRAIN NEOPLASMS: EXPERIENCE WITH 106 CASES

A thesis submitted to the University of Arizona College of Medicine – Phoenix
in partial fulfillment of the requirements for the Degree of Doctor of Medicine

Alessandro Carotenuto
Class of 2019

Mentor: Mark C. Preul, MD

Acknowledgements

This research was supported with funds from the Barrow Neurological Foundation, the Women's Board of the Barrow Neurological Institute, and by the Newsome Chair in Neurosurgery Research held by Dr. Preul. We thank Carl Zeiss Meditec, Inc., Dublin, CA, USA, for providing the LSM 710 microscope. Dr. Belykh is supported by the scholarship SP-2240.2018.4. Authors are thankful to the Neuropublications Department of the Barrow Neurological Institute for editorial support with figures and video supplement.

Abstract

Objectives

Frozen section histological analysis is currently the mainstay for intraprocedural tissue diagnosis during the resection of intracranial neoplasms and for evaluating tumor margins. However, frozen sections are time-consuming and often do not reveal the histological features needed for final diagnosis when compared with permanent sections. Confocal scanning microscopy (CSM) with certain stains may be a valuable technology that can add rapid and detailed histological assessment advantage for the neurosurgical operating room. This study describes potential advantages of CSM imaging of fresh human brain tumor tissues labeled with acriflavine (AF), acridine orange (AO), cresyl violet (CV), methylene blue (MB), and indocyanine green (ICG) within the neurosurgical operating room facility.

Patients and methods

Acute slices from orthotopic human intracranial neoplasms were incubated with AF/AO and CV solutions for 10 s and 1 min respectively. Staining was also attempted with MB and ICG. Samples were imaged using a bench-top CSM system. Histopathologic features of corresponding CSM and permanent hematoxylin and eosin images were reviewed for each case.

Results

Of 106 cases, 30 were meningiomas, 19 gliomas, 13 pituitary adenomas, 9 metastases, 6 schwannomas, 4 ependymomas, and 25 other pathologies. CSM using rapid fluorophores (AF, AO, CV) revealed striking microvascular, cellular and subcellular structures that correlated with conventional histology. By rapidly staining and optically sectioning freshly resected tissue, images were generated for intraoperative consultations in less than one minute. With this technique, an entire resected tissue sample was imaged and digitally stored for tele-pathology and archiving.

Conclusion

CSM of fresh human brain tumor tissue provides clinically meaningful and rapid histopathological assessment much faster than frozen section. With appropriate stains, including specific cellular structure or antibody staining, CSM could improve the timeliness of intraoperative decision-making, and the neurosurgical-pathology workflow during resection of human brain tumors, ultimately improving patient care.

Table of Contents

List of Tables and Figures

Introduction

It is estimated that nearly 78,000 people in the U.S. develop brain and central nervous system neoplasms each year [1]. Initial work up of these lesions often includes stereotactic biopsy to identify histological diagnosis and further management [2]. Certainly, the intraoperative histology guides resection strategy and optimizes tissue banking [3,4]. Frozen sections are the current gold standard for intraoperative diagnosis and are small biopsy specimens often sent initially from the main tumor mass, and then from the suspected tumor boundary region as the surgery progresses. Frozen section histology usually correlates with analysis of the tissue for permanent histology for final diagnosis [4]. However, the diagnostic discrepancy between frozen and permanent sections is reported to be as high as 2.7% [5]. Frozen section histology implements only simple staining techniques and requires 15–40 min of processing time [6]. Freezing or cautery artifacts can affect the diagnostic accuracy [7]. Artifacts and sampling error reduce diagnostic yield and often require harvest of additional biopsy specimens, which significantly increases surgery and anesthesia times.

Confocal scanning microscopy (CSM) has become an accepted, powerful, standard research technique for investigations into tumor cell biology. Samples can be imaged utilizing a variety of specific and non-specific fluorophores or intrinsic tissue fluorescence [[8], [9], [10], [11]]. This technology would seem to be well poised to be propitiously adopted into dedicated clinical use, especially for neurosurgical tumor procedures. So far, however, the high equipment cost and requirement for specialists versed in CSM imaging has impeded wide implementation of this technology in clinical settings [12].

Unlike frozen sections, fresh tissue samples near immediately stained with rapid-acting fluorophores are not affected with freezing artifacts and do not require a lengthy period of tissue preparation [13]. Utilization of rapid-acting fluorophores could significantly reduce the time needed to provide feedback during intraoperative histopathological consultation, improve intraoperative decision-making, and potentially reduce surgery and anesthesia times [10,13,14].

The goal of this article is to describe and assess performance and feasibility of CSM to image fresh human brain tumor tissue biopsies labeled with rapid staining fluorophores within the time of surgery. The fluorophores used in this study were chosen because they provide immediate staining of the tissue, thus minimizing the time between intraoperative tissue harvest and histologic data acquisition [10,11,13,14].

Materials and methods

This study was approved by the Institutional Review Board at the Barrow Neurological Institute, St. Joseph's Hospital and Medical Center. Patients with intracranial neoplasms requiring craniotomy for surgical resection were eligible for the study. Over a sequential 6-month period, 106 patients were prospectively enrolled in this study. The exclusion criteria included age younger than 18 years and inability to sign informed consent.

2.1. Tissue sampling

Intraoperative image-guided neurosurgical technique was used in all patients (StealthStation Surgical Navigation, Medtronic, Inc., Dublin, Ireland). All enrolled patients underwent craniotomy. The dura was opened and an approach to the tumor was performed. Standard microsurgical biopsy technique was used to harvest tissue samples from areas corresponding with contrast enhancement on co-localized contrast-enhanced T1-weighted MRI images [13,14]. Tissue samples were stored in vials containing ice-cold artificial cerebrospinal fluid to ensure preservation of the viable tissue. Artificial cerebrospinal fluid contained the following components (in mM): 126 NaCl, 26 $NaHCO_3$, 2.5 KCl, 1.25 NaH_2PO_4, 2 $MgSO_4$, 2 $CaCl_2$ and 10 glucose, pH 7.4 [15]. Samples were transferred to the pathology department for imaging with the CSM. There were a total of 6 samples from each patient (approximate volume 0.25 cm^3 each). Each sample was placed into a No 1.5 glass bottom dish (MatTek, Ashland, MA) for CSM imaging (Fig. 1).

2.2. Fluorophores

Rapid-staining fluorophores selected for this study were: acriflavine hydrochloride (AF), acridine orange (AO), cresyl violet (CV), methylene blue (MB), indocyanine green (ICG) (Table 1). A control sample was imaged without addition of fluorophores from each patient. The optimal staining time was calculated for each fluorophore. These fluorophores were selected because our group has had significant experience with their use in confocal laser endomicroscopy of brain tumor tissue and because of their convenient employment for CSM [10,13,14,16].

2.3. Confocal scanning microscopy

CSM was performed with a Zeiss LSM 710/5Live DUO system (Carl Zeiss AG, Oberkochen, Germany). A set of 3 images was taken with different magnifications (24×, 40× and 60×) for each sample. In addition, large simulated low-magnification images were acquired from the samples and sequential images were transformed into digital image video loops. Fluorophore-labeled samples were placed onto the motorized stage of the CSM equipped with a 40×/1.2NA water emersion objection. Acriflavine, AO, CV, MB, and ICG were imaged with the following excitation/full width at half maximum emission spectra respectively: 405/545 nm, 489/615 nm, 561/684 nm, 633/707 nm and 635/670 nm. The confocal aperture was set to one Airy unit for all imaging. The laser and gain values were set to fill the dynamic range of the photomultiplier tubes, and the frame size was set to sample at Nyquist. Images were collected in 8- and 12-bit format absent of non-linear processing. Simulated low magnification images were acquired by adjusting the digital zoom to 24× and 900 μm2 fields of view were collected with automated image tilling. In some cases, images from entire samples were rapidly tiled and optically sectioned using a Zeiss line-sweeping CSM. Frame size for this system was fixed to 512 × 512 by a linear charged coupled device (CCD) array. The total imaging time was calculated for each sample and patient.

2.4. Histology and data processing

Imaging sites of the tissue samples were marked with ink to obtain matched CSM and conventional histological sections. Samples were placed into the tissue cassette for further formalin fixation and paraffin embedding. Ten micrometer tissue sections were obtained for hematoxylin and eosin staining (H&E) and light microscopy. Matched CSM images and permanent sections were reviewed by a group of 2 neuropathologists and 3 neurosurgeons. The cytoarchitecture and histopathologic features were identified and compared between CSM images and H&E. Data analysis was performed with Microsoft Excel (Microsoft Corp., Redmond, WA).

Fig. 1. Tissue sampling and imaging set up. (A) Tissue samples embedded in (left to right) AF, ICG, CV, AO, artificial cerebrospinal fluid. (B) Setup of the confocal microscope. Used with permission from Barrow Neurological Institute, Phoenix, Arizona, USA.

Table 1
Fluorophores used in the study, their properties and observed quality of tissue staining.

Fluorophore	Cell Permeability	Excitation/ Emission (nm)	Fluorescence Localization	Concentration Providing Best Image Quality	Other Concentrations Used	Qualitative Fluorescence Intensity	Qualitative Structural Clarity
AO	yes	488/505–700	DNA/RNA/ lysosome	0.01%	0.05%, 0.001%	Good	Good
AF	yes	405/505–585	membrane/DNA	0.05%	0.1%, 0.01%	Good	Good
CV	yes	561/620–655	ER/cytoplasm	0.02%	0.002%	Moderate	Moderate
MB	yes	665/685	DNA	82%	8.2%	Low	Low
ICG	yes	778/700-850	Cytoplasm/proteins	0.6%	0.12%, 0.06%	Low	Low

Results

One-hundred and six consecutive patients (48 females and 58 males) were prospectively enrolled in this study with mean age of 53 years (range 18–84). Each patient had a total of six samples imaged with a variety of fluorophores. There were 1960 CSM images acquired in this study (19 images per patient). Total imaging time was 20 min per patient. Average time from specimen arrival to the pathology department to obtaining the first CSM image was one minute. Average time to obtain frozen sections results in this study was 15 minutes from the specimen arrival to the pathology department. CSM images were saved as video loops in digital format and could be electronically transferred to an offsite neuropathologist within a few minutes (Supplemental Video 1).

3.1. Fluorophores

AF and AO provided instant fluorescence with high clarity and contrast of histopathologic features. Because of that characteristic, AF and AO-stained samples were imaged first. Both AF and AO produced high-quality staining of extracellular and intracellular structures, predominantly nuclei and cellular membranes revealing detailed images. However, AF had a propensity to label more extracellular structures than AO. In some cases, AF obscured interpretation of the intracellular structures. AF and AO provided good quality fluorescence in all cases, except for cavernous malformations.

CV staining generated an optimal fluorescent appearance within five to six minutes. Unlike AF and AO that stained nuclei primarily, CV caused diffuse fluorescence of the cytoplasm that highlighted large diffuse areas of the image. Cell morphology was defined by fluorescent cytoplasm encased within the cell membrane; intracellular components were identified as dark silhouettes over bright fluorescent cytoplasm. CV provided high quality images, however nucleoli were not identifiable compared with AO or AF stains.

MB and ICG exhibited minimal fluorescence with the described staining procedures and imaging techniques. No meaningful histopathological patterns were identified.

One sample from each patient was imaged using the described CSM imaging parameters, but without addition of fluorophores. The identified auto fluorescence was minimal and did not overlap with signals associated with any of the fluorophores.

3.2. Histopathology

The final diagnoses in the cases in this study included: 30 meningiomas (World Health Organization [WHO] Grade I [n = 28], II [n = 2]), 19 gliomas (WHO Grade II [n = 5], Grade III [n = 3], and Grade IV [n = 11]). The rest of the 57 cases included 13 pituitary adenomas, nine metastases, seven cavernous malformations, six schwannomas, five subependymomas, four ependymomas, three radiation necroses/gliosis and one each for chordoma, craniopharyngioma, fibrous dysplasia, hemangiopericytoma, primary CNS lymphoma, nerve sheath tumor, neurocytoma, paraganglioma, pleomorphic xanthoastrocytoma, squamous cell carcinoma (Table 2).

Meningiomas were best visualized with AF and AO staining. The quality of CV staining was not consistent. Amongst 30 meningiomas 13 were transitional, nine meningothelial, two atypical, four fibrous, and two secretory. Meningiomas stained with AF and AO demonstrated whorls of oval to spindled cells with various amounts of pericellular collagen proliferating in a vesicular pattern. Psammoma bodies could be seen in multiple cases. Secretory meningiomas had characteristic secretory inclusions and cytoplasmic laminae. Atypia was apparent in WHO Gr II meningiomas. The correct diagnosis and subtype could be identified in 26 cases (86.7%). In three cases (10%) (fibrous and meningothelial meningiomas) it was possible to identify meningioma although subtyping was not accurate. In one case (transitional meningioma) the diagnosis could not be identified due to poor image quality (Fig. 2).

Gliomas were better visualized with AF and AO staining. Staining with CV did not provide reliable histological information in all cases, although based on CV staining in anaplastic oligodendrogliomas, mitotic figures, microvascular proliferation, and tumor necrosis were identifiable. Hypercellularity with diffuse parenchymal infiltration and dystrophic calcifications with adjacent intermingled tumor cells were readily noted. Tumor cells had round to oval nuclei

and apparent fibrillary processes. Atypical features were also visualized. The correct diagnosis of glioma was made in 17 of 19 cases (89.0%). The correct subtyping was possible in four cases (21.0%) (three glioblastomas, one oligodendroglioma). In two cases (glioblastoma, oligodendroglioma) the diagnosis could not be identified due to poor image quality (Fig. 3). Treatment effect presented as large areas of pseudonormal brain tissue pattern showing non-neoplastic reactive changes with high macrophage content.

Pituitary adenomas demonstrated sheets of round to oval cells with prominent nuclei and a moderate amount of bright cytoplasm with CV. Normal pituitary cells appeared smaller with less pleomorphic nuclei than neoplastic pituitary epithelial cells with AO and AF. The correct diagnosis could be determined for all pituitary adenoma cases in this study (n = 13).

There were nine cases of metastatic disease in this series (six adenocarcinomas, three carcinomas). These lesions were optimally stained with AO and AF. Fluorescence in adenocarcinomas showed sheets of cells with or without gland formation. Atypical cells contained rich bright cytoplasm with secretory granules. In cases with gland formation, there was necrotic debris filling the gland. In one case of metastatic clear cell carcinoma, invading cells with prominent clear cytoplasm were noted. Correct diagnosis was possible in five of nine cases (four metastatic adenocarcinomas, one metastatic carcinoma) (55.6%). In the remaining four cases, although atypical cells were identified, correct diagnosis was not possible with CSM imaging.

Schwannomas represented six cases in this study. Staining with AO and AF provided informative images that correlated with conventional H&E. In all cases spindled cells and nuclei were apparent. Antoni A and B areas were identified in all cases. In two cases verocay bodies were apparent. Correct diagnosis was made in all six cases (Fig. 4).

Subependymomas staining revealed clusters of isomorphic nuclei embedded in a dense, fine, glial fibrillary background. They were best identified with AF, however, AO also provided important complimentary histopathologic data. Of five cases, correct diagnosis was possible

only in three (60%). In the remaining two cases, although atypical cells were identified, the correct diagnosis was not possible because of insufficient histopathologic data.

Ependymoma fluorescence appearance showed cells with round to oval nuclei with only mild atypia. There was distinct arrangement of tumor cells into perivascular pseudorosettes in one case. AF and AO provided the most informative histopathologic information. Correct diagnosis was possible in only one case (25%). In three cases (75%), atypical cells were identified, but histopathologic information derived from CSM images was not sufficient to determine the diagnosis.

A central neuroctyoma revealed proliferation of neoplastic cells arranged in diffuse sheets and nests and was best visualized with AF and AO (Fig. 5). The tumor cells were embedded in a background of fine fibrillary stroma. The individual cells demonstrated round nuclei with fine chromatin. Mitotic figures were not identified.

Squamous cell carcinoma presented as multiple nests of infiltrating moderately differentiated squamous carcinoma with scattered mitosis and was best visualized with AF and AO. Tumor cells had atypical large nuclei and abundant cytoplasm.

Cavernous malformations did not exhibit an informative fluorescent histologic pattern with any fluorophore used in this study.

There were 99 patients with true neoplastic or related processes in this study seven cases of cavernous malformations were not included in this analysis). In 66 cases (66.7%) CSM correctly identified the diagnosis including tumor subtype when compared to conventional histopathologic analysis (Table 3). In five patients (5.1%) CSM images did not contain useful diagnostic information (Table 4). In 28 patients (28.3%) CSM identified a neoplastic process, however subtyping was not possible (Table 5). Overall CSM detected neoplastic process in 94 patients (95%).

3.3. Volumetric imaging

CSM can scan the entire tissue sample by shifting the field of view. In addition, virtual image slices along the Z-axis allowed volumetric analysis of the tissue. We scanned with the 488 nm laser range to a depth of about 50 µm. Also, CSM allowed increase or decrease of magnification for more detailed analysis of the tumor cells or area of interest and navigation software allowed review and recovery of various imaging locations to study meaningful tissue or cell characteristics.

Table 2. Frequency of histopathologies in this study

	Number of patients
Meningioma	30
Glioma	19
Pituitary adenoma	13
Metastasis	9
Cavernous malformation	7
Schwannoma	6
Subependymoma	5
Ependymoma	4
Radiation necrosis	2
Chordoma	1
Craniopharyngioma	1
Gliosis	1
Fibrous dysplasia	1
Hemangiopericytoma	1
Primary CNS lymphoma	1
Nerve sheath tumor	1
Neurocytoma	1
Paraganglioma	1
Pleomorphic xanthoastrocytoma	1
Squamous cell carcinoma	1

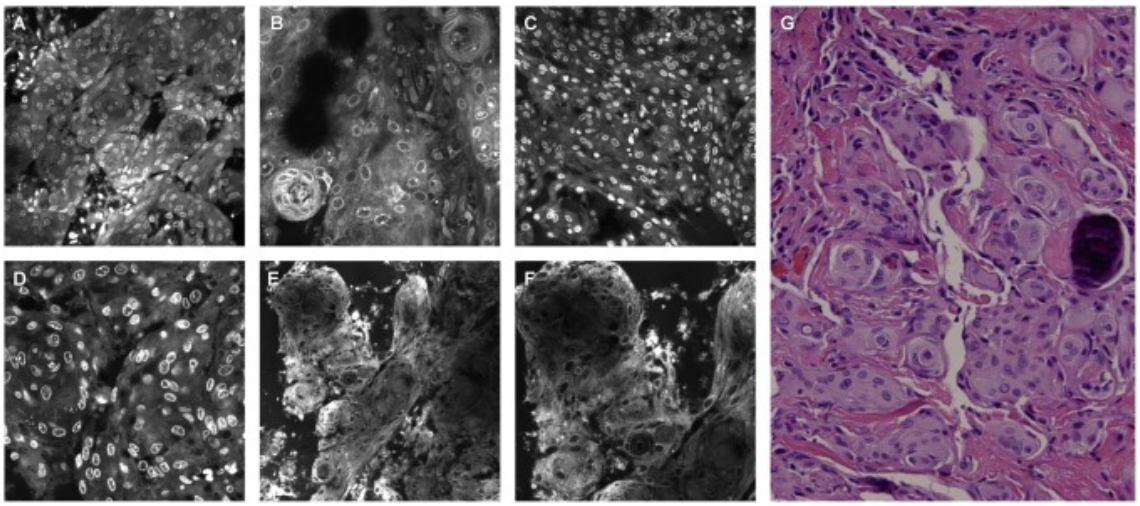

Fig. 2. Meningothelial meningioma. Ex vivo confocal images (A–F) obtained in case meningothelial meningioma. (A, B) stained with AO, (C, D) stained with AF, (E, F) stained with CV. (G) photomicrograph of H & E–stained sections showing histopathological features of whorls, psammoma bodies, and collagen similar to those of the matched imaging location. Original magnification ×200 (A, C, E, G) and ×400 (B, D, F). Used with permission from Barrow Neurological Institute, Phoenix, Arizona, USA.

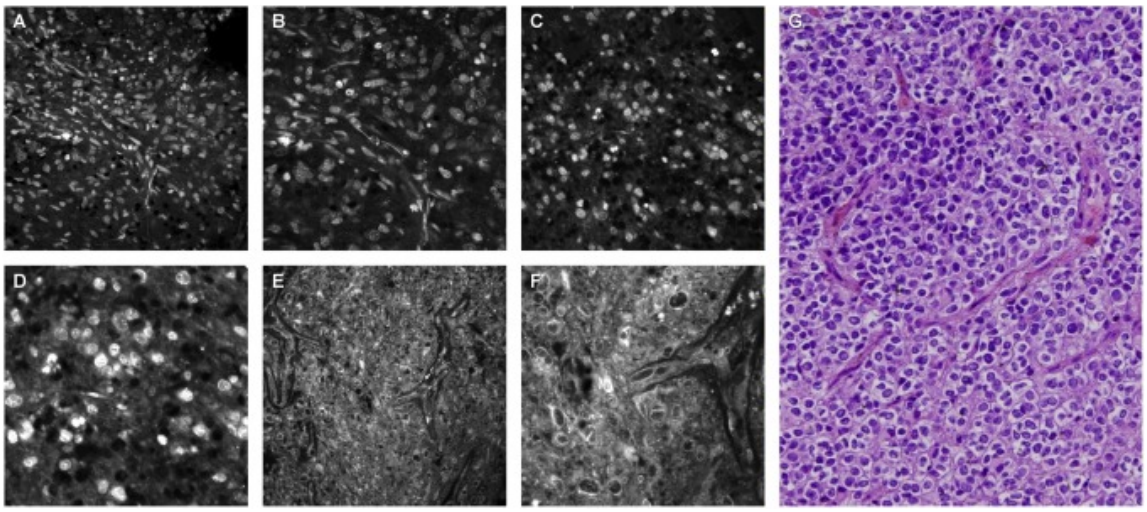

Fig. 3. Glioblastoma. Ex vivo confocal images (A–F) obtained in case glioblastoma. (A, B) stained with AO, (C, D) stained with AF, (E, F) stained with CV. (G) photomicrograph of H & E–stained sections showing histopathological features of cellular tumor with hypercellularity, atypia, and neovascularization similar to those of the matched imaging location. Original magnification ×200 (A, C, E, G) and ×400 (B, D, F). Used with permission from Barrow Neurological Institute, Phoenix, Arizona, USA.

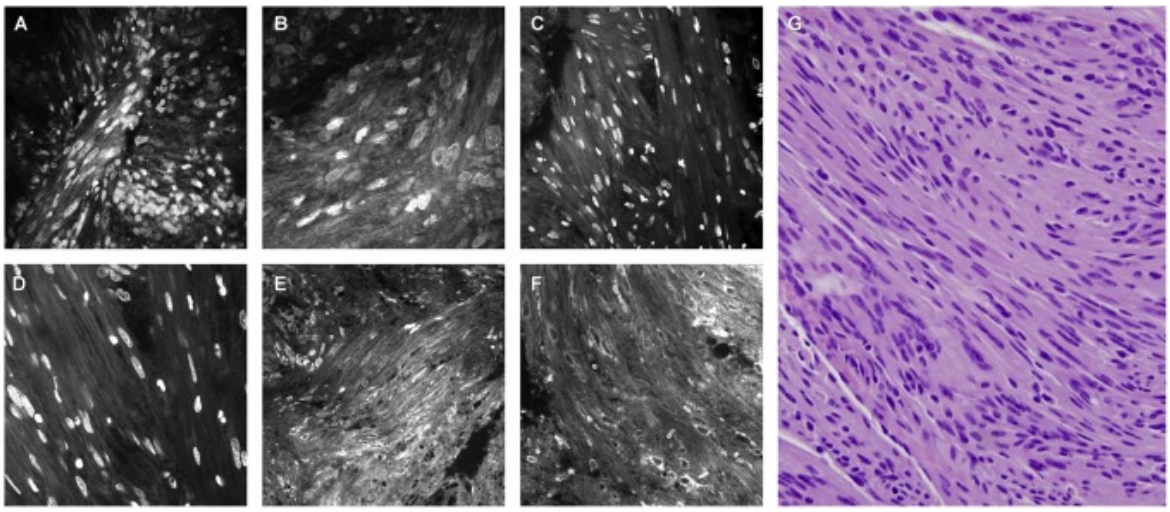

Fig. 4. Schwannoma. Ex vivo confocal images (A–F) obtained in case glioblastoma. (A, B) stained with AO, (C, D) stained with AF, (E, F) stained with CV. (G) photomicrograph of H & E–stained sections showing histopathological features of cellular tumor with fascicles of cells with elongated cytoplasmic processes. Original magnification ×200 (A, C, E, G) and ×400 (B, D, F). Used with permission from Barrow Neurological Institute, Phoenix, Arizona, USA.

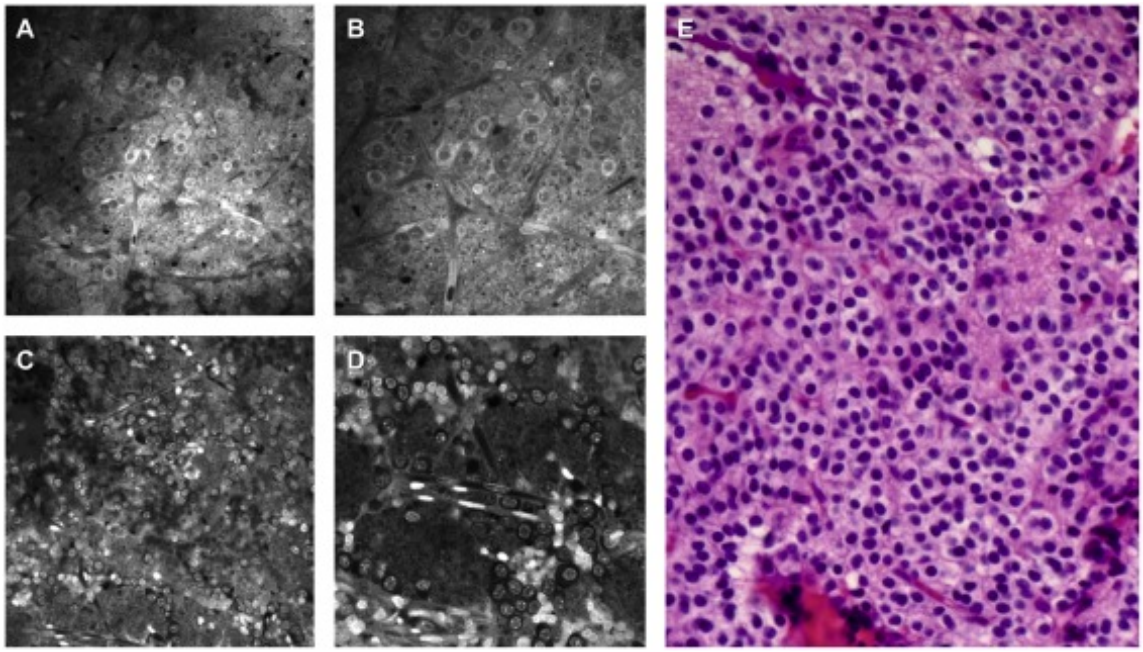

Fig. 5. Central neurocytoma. Ex vivo confocal images (A–D) obtained in case glioblastoma. (A, B) stained with AO, (C, D) stained with AF. (E) photomicrograph of H & E–stained sections showing histopathological features tumor cells embedded in a background of fine fibrillary stroma. The individual cells demonstrate round nuclei. Original magnification ×200 (A, C, E) and ×400 (B, D). Used with permission from Barrow Neurological Institute, Phoenix, Arizona, USA.

Table 3. Diagnostic accuracy in most common histopathological types

	Accurate diagnosis		Tumor, no subtyping		No diagnostic images		Total number of cases
	n	%	n	%	n	%	
Meningioma	26	87%	3	10%	1	3%	30
Glioma	4	21%	13	68%	2	11%	19
Pituitary adenoma	13	100%	0	0%	0	0%	13
Metastasis	5	56%	4	44%	0	0%	9
Cavernous malformation	0	0%	0	0%	7	100%	7
Schwannoma	6	100%	0	0%	0	0%	6
Subependymoma	3	60%	2	40%	0	0%	5
Ependymoma	3	75%	1	25%	0	0%	4

Table 4. Cases with no diagnostic images

Cases with no diagnostic images	**Number of cases**
Cavernous malformation	7
Oligodendroglioma	1
Glioblastoma	1
Transitional meningioma	1
Craniophryngioma adamantinous	1
Fibrous dysplasia	1

Table 5. Cases with images with distinguishable tumor. No subtyping possible.

Cases with distinguishable tumor, no subtyping possible	**Number of cases**
Glioblastoma	7
Oligodendroglioma	3
Ependymoma	3
Metastatic colon carcinoma	2
Subependymoma	2
Fibrous meningioma	1
Meningothelial meningoioma	1
Transitional meningioma	1
Anaplastic oligodendroglima	2
Anaplastic astrocytoma	1
Metastatic poorly differentiated adenocarcinoma	1
Metastasis lung adenocarcinoma	1
Paraganglioma	1
Primary CNS lymphoma	1
Hemangiopericytoma	1

Discussion/Future Direction

This study assesses the feasibility of CSM as a dedicated imaging platform that is aimed at consistently augmenting a neurosurgical oncology and pathology workflow. Fluorescent microscopy technologies have been actively studied to improve precision of surgery and complement histological analysis of biopsies. Although CSM technology can be considered as a forerunner of the handheld confocal laser endomicroscopes, the utility and resultant image quality of CSM has not been previously investigated in the neurosurgery operating room [17]. Our results therefore define a baseline of performance, feasibility, and diagnostic accuracy for CSM when applied in a clinical setting compared to what has been achieved on brain tumor tissue with the standard research grade benchtop CSM technology in the laboratory.

4.1. Appearances of the fluorophores with pathology types

Traditionally, CSM has been used for research applications [18,19]. High costs for purchase and technician operation in comparison to light microscopes seem to have prohibited widespread use of CSM into routine clinical practice. This study describes utility of a benchtop CSM system for rapid acquisition of fluorescent histologic information during neurosurgical tumor removal procedures using non-specific and specific fluorescent stains. While this experience is preliminary, identifying specific utility and cellular structure appearance for each fluorophore may improve workflow during intracranial neoplasm surgery. The variety of rapid-staining fluorophores examined for this study allows for identification and differentiation of histopathologic features. Flow of information from fluorescence staining of fresh tissue combined with benchtop CSM imaging was significantly faster compared to the conventional “frozen sections” method of initial tumor tissue assessment.

In this study, rapidly staining fluorophores were utilized: AO, AF, CV, ICG, and MB. AO and AF stained tissue instantaneously, while CV required a stain time of 5–6 min and revealed a detailed unique histologic appearance for pituitary adenomas. Many of these dyes can be used in vivo for example during gastrointestinal and bronchoscopy procedures, but they cannot be

used in the live human brain [20,21]. Ex vivo imaging allows for use of an expanded repertoire of fluorophores on brain tissue, many of which are considered too toxic for in vivo use.

A histologically meaningful fluorescence was not detected with MB or ICG at the concentrations and imaging parameters used in these experiments. The majority of CSMs are not equipped for infrared imaging. Therefore, imaging MB/ICG stained samples was performed with far-red imaging parameters, although MB/ICG did not produce useful images with CSM at these parameters either. ICG delineation of tumor cells can be seen with microscopy systems operating in the near-infrared laser range [11,[22], [23], [24], [25]].

Cavernous malformations did not stain with fluorophores used in this study. This could be explained by the biostructural properties of cavernous malformations. Cavernous malformations are not neoplasms and hypercellularity with atypia is not characteristic for these lesions [26,27]. Thus, they did not exhibit fluorescence patterns as observed for the neoplastic lesions investigated in this study.

4.2. Acquisition of fluorescent signal

The histopathologic features obtained with CSM were accurate and easily recognized in 66.7% of tumor cases when compared with conventional methods of clinical histology. The imaging parameters and fluorophores used in this study allowed acquisition of extremely high resolution images producing detail at multiple magnifications. Lower magnifications were useful to assess tissue cytoarchitecture, while higher magnification facilitated analysis of intracellular components. The CSM was capable of imaging the entire specimen quickly and allowed high-magnification visualization at any chosen area. These data could be stored and transmitted as still images and digital video loops. This imaging process can be simplified and automated, which could be useful for telepathology.

In 30.3% cases where precise diagnosis was not possible, CSM images provided confirmation of a neoplastic process. In most of these cases the tissue sample was not large enough for CSM imaging with the variety of fluorophores. This situation resulted because of the small size of the primary lesion, where the priority was made to provide enough tissue for clinical diagnosis via

conventional histopathology. Although the appearance of images stained with such fluorophores reveals images different from conventional H&E or other stains, already many neuropathologists are becoming experienced with assessment of images from CSM systems and likewise are gaining experience with images from confocal laser endomicroscopy of ex vivo and in vivo brain and other organ tissue [10,[13], [14], [15],24].

4.3. Clinical application of confocal scanning microscopy

Widespread adoption of CSM technology would require demonstrating utility and establishing a CSM platform that is refined and dedicated for clinical pathology use [28,29]. In our experience, the use of CSM significantly decreased the time duration to acquire histopathologic data in comparison with frozen sections [14]. In our series, CSM accurately detected a neoplastic process in 95% of cases within 1 min after the specimen arrived to pathology department. Results of our study with CSM are in line with previous reports that used other technologies including hand held confocal laser endomicroscopy for ex vivo human and animal tumor tissue staining, and also application of novel Raman microscopes for stainless tissue imaging [10,[30], [31], [32]]. Although confocal laser endomicroscopy is being investigated for its portable on-the-fly performance within the surgical site, benchtop CSM technology can image the tissue specimen with a range of multiple lasers and produces comparatively better quality images.

A CSM platform such as the system used in this study provides a wealth of powerful tissue analytic techniques that can add substantial cellular information over a relatively brief time, although not generally within the very few minutes demanded by intraoperative reporting currently. These applications include volumetric imaging, with depth of imaging determined by the laser characteristics and the tissue (in our study to about 50 μm at 488 nm). However, penetration into the tissue can approach 1 mm with non-linear optics add-ons that combine multiphoton capabilities with CSM [33,34]. Another potential improvement towards clinical use is application of spinning-disk technology, which increases the image acquisition speed from below video rate (<30 frames per second) for CSM to 200–1000 frames per second, allowing for instant video-like imaging at high resolution [35]. The trend is really towards providing a more representative and accurate imaging session for tissues in vivo [14,36,37] or rapidly ex vivo

[38,39] that also involves analyzing the interactions of structures. CSM navigation software allows the user to move throughout the tissue, and to quickly recover locations of tissue interest. Other capabilities that may require longer duration include photobleaching and photoactivation experiments that are relevant for cancer tissue examination, including cell death, analysis of DNA repair proteins, protein synthesis or detailed mechanisms of cell division. Additionally, CSM can simultaneously image multiple fluorescent dyes and single molecules can be imaged rapidly with advanced modules such as fluorescence correlation spectroscopy and image correlation spectroscopy [40]. Lastly, highly functional and integrated image processing software can provide new dimensions in terms of tissue examination and display.

Conclusions

In the setting of intracranial biopsy, qualified use of CSM with appropriate fluorophores would be sufficient to analyze tissue and complete the procedure without additional sampling and could help to reduce operating room and anesthesia time for biopsy procedures. This could be implemented across clinical specialties beyond neurosurgery, e.g., for sentinel lymph node biopsy. In the setting of a multispecialty hospital where there are multiple such procedures performed daily, the economies of scale could exist to make it worthwhile for hospitals to adopt such technology. Very likely, the simplification of a research CSM system specifically adapted and dedicated for clinical histological imaging could potentially decrease the price per unit. While the fluorescent dyes we used in this study can provide additional and alternative histological data, application of specific labels for tissue acquired from the operating room that can be rapidly processed and visualized in the pathology laboratory will yield improved intraoperative diagnosis and influence surgical decisions. It would seem likely that CSM technology will be developed and refined providing more efficient machine operation and analysis that may be adapted for the operating room. Such technology would add a near-immediate parameter to tissue assessment for imaging of various cell structures and detection of relevant specific prognostic markers as seen in the laboratory.

References

1. Ostrom QT, Gittleman H, Fulop J, et al. CBTRUS Statistical Report: Primary Brain and Central Nervous System Tumors Diagnosed in the United States in 2008-2012. *Neuro Oncol.* Oct 2015;17 Suppl 4:iv1-iv62.
2. Ryu S, Buatti JM, Morris A, et al. The role of radiotherapy in the management of progressive glioblastoma : a systematic review and evidence-based clinical practice guideline. *J Neurooncol.* Jul 2014;118(3):489-499.
3. Shabihkhani M, Lucey GM, Wei B, et al. The procurement, storage, and quality assurance of frozen blood and tissue biospecimens in pathology, biorepository, and biobank settings. *Clin Biochem.* Mar 2014;47(4-5):258-266.
4. Jaafar H. Intra-operative frozen section consultation: concepts, applications and limitations. *Malays J Med Sci.* Jan 2006;13(1):4-12.
5. Plesec TP, Prayson RA. Frozen section discrepancy in the evaluation of central nervous system tumors. *Arch Pathol Lab Med.* Oct 2007;131(10):1532-1540.
6. Nordrum I, Engum B, Rinde E, et al. Remote frozen section service: a telepathology project in northern Norway. *Hum Pathol.* Jun 1991;22(6):514-518.
7. Chatterjee S. Artefacts in histopathology. *J Oral Maxillofac Pathol.* Sep 2014;18(Suppl 1):S111-116.
8. Belykh E, Martirosyan NL, Yagmurlu K, et al. Intraoperative Fluorescence Imaging for Personalized Brain Tumor Resection: Current State and Future Directions. *Front Surg.* 2016;3:55.
9. Georges J, Zehri A, Carlson E, et al. Label-free microscopic assessment of glioblastoma biopsy specimens prior to biobanking [corrected]. *Neurosurg Focus.* Feb 2014;36(2):E8.
10. Martirosyan NL, Georges J, Eschbacher JM, et al. Potential application of a handheld confocal endomicroscope imaging system using a variety of fluorophores in experimental gliomas and normal brain. *Neurosurg Focus.* Feb 2014;36(2):E16.
11. Martirosyan NL, Cavalcanti DD, Eschbacher JM, et al. Use of in vivo near-infrared laser confocal endomicroscopy with indocyanine green to detect the boundary of infiltrative tumor. *J Neurosurg.* Dec 2011;115(6):1131-1138.

12. Zucker RM, Chua M. Evaluation and purchase of confocal microscopes: numerous factors to consider. *Curr Protoc Cytom.* Oct 2010;Chapter 2:Unit2 16.
13. Martirosyan NL, Eschbacher JM, Kalani MY, et al. Prospective evaluation of the utility of intraoperative confocal laser endomicroscopy in patients with brain neoplasms using fluorescein sodium: experience with 74 cases. *Neurosurg Focus.* Mar 2016;40(3):E11.
14. Eschbacher J, Martirosyan NL, Nakaji P, et al. In vivo intraoperative confocal microscopy for real-time histopathological imaging of brain tumors. *J Neurosurg.* Apr 2012;116(4):854-860.
15. Charalampaki P, Javed M, Daali S, Heiroth HJ, Igressa A, Weber F. Confocal Laser Endomicroscopy for Real-time Histomorphological Diagnosis: Our Clinical Experience With 150 Brain and Spinal Tumor Cases. *Neurosurgery.* Aug 2015;62 Suppl 1:171-176.
16. Wirth D, Snuderl M, Curry W, Yaroslavsky A. Comparative evaluation of methylene blue and demeclocycline for enhancing optical contrast of gliomas in optical images. *J Biomed Opt.* Sep 2014;19(9):90504.
17. Snuderl M, Wirth D, Sheth SA, et al. Dye-enhanced multimodal confocal imaging as a novel approach to intraoperative diagnosis of brain tumors. *Brain Pathol.* Jan 2013;23(1):73-81.
18. Wirth D, Snuderl M, Sheth S, et al. Identifying brain neoplasms using dye-enhanced multimodal confocal imaging. *J Biomed Opt.* Feb 2012;17(2):026012.
19. Mosnier JF, Brunon J, Nuti C. [Histopathology of central nervous system cavernomas]. *Neurochirurgie.* Jun 2007;53(2-3 Pt 2):131-135.
20. Cavalcanti DD, Kalani MY, Martirosyan NL, Eales J, Spetzler RF, Preul MC. Cerebral cavernous malformations: from genes to proteins to disease. *J Neurosurg.* Jan 2012;116(1):122-132.
21. Foldes-Papp Z, Demel U, Tilz GP. Laser scanning confocal fluorescence microscopy: an overview. *Int Immunopharmacol.* Dec 2003;3(13-14):1715-1729.
22. Combs CA, Shroff H. Fluorescence Microscopy: A Concise Guide to Current Imaging Methods. *Curr Protoc Neurosci.* Apr 10 2017;79:2 1 1-2 1 25.

23. Wirth D, Smith TW, Moser R, Yaroslavsky AN. Demeclocycline as a contrast agent for detecting brain neoplasms using confocal microscopy. *Phys Med Biol.* Apr 07 2015;60(7):3003-3011.
24. Mooney MA, Georges J, Yazdanabadi MI, et al. Immediate ex-vivo diagnosis of pituitary adenomas using confocal reflectance microscopy: a proof-of-principle study. *J Neurosurg.* May 26 2017:1-4.